Received: 24 March 2020 | Revised: 29 July 2020 | Accepted: 5 August 2020

DOI: 10.1002/ijc.33262

MOLECULAR CANCER BIOLOGY

IJC International Journal of Cancer

Loss of the cystine/glutamate antiporter in melanoma abrogates tumor metastasis and markedly increases survival rates of mice

Mami Sato[1,2,3] | Kunishige Onuma[4,5] | Mio Domon[1] | Shun Hasegawa[1] | Ami Suzuki[1] | Ryosuke Kusumi[1] | Remi Hino[1] | Nahoko Kakihara[6] | Yusuke Kanda[4] | Mitsuhiko Osaki[4,7] | Junichi Hamada[8] | Shiro Bannai[1] | Regina Feederle[9] | Katalin Buday[3] | José Pedro Friedmann Angeli[10] | Bettina Proneth[3] | Marcus Conrad[3,11] | Futoshi Okada[4,7] | Hideyo Sato[1]

[1]Laboratory of Biochemistry and Molecular Biology, Department of Medical Technology, Faculty of Medicine, Niigata University, Niigata, Japan

[2]Sakeology Center, Niigata University, Niigata, Japan

[3]Helmholtz Zentrum Muenchen, Institute of Metabolism and Cell Death, Neuherberg, Germany

[4]Division of Experimental Pathology, Tottori University Faculty of Medicine, Yonago, Japan

[5]Department of Clinical Bio-resource Research and Development, Graduate School of Medicine Kyoto University, Kyoto, Japan

[6]Department of Nursing, Faculty of Medicine, Niigata University, Niigata, Japan

[7]Chromosome Engineering Research Center, Tottori University, Yonago, Japan

[8]Health Sciences University of Hokkaido, School of Nursing and Social Services, Ishikari, Tobetsu, Japan

[9]Helmholtz Zentrum Muenchen, Institute for Diabetes and Obesity, Monoclonal Antibody Core Facility, Neuherberg, Germany

[10]Rudolf Virchow Center for Translational Bioimaging, University of Wuerzburg, Wuerzburg, Germany

[11]National Research Medical University, Laboratory of Experimental Oncology, Moscow, Russia

Correspondence
Hideyo Sato, Laboratory of Biochemistry and Molecular Biology, Department of Medical Technology, Faculty of Medicine, Niigata University, 746-2 Asahimachi-dori, Chuo-ku, Niigata 951-8518, Japan.
Email: hideyo-s@clg.niigata-u.ac.jp

Funding information
Deutsche Forschungsgemeinschaft, Grant/Award Numbers: CO 291/5, FR 3746/3-1; Interdisziplinäres Zentrum für Klinische Forschung, Universitätsklinikum Würzburg, Grant/Award Number: B424; Japan Society for the Promotion of Science (JSPS KAKENHI), Grant/Award Number: JP17K07158

Abstract

The cystine/glutamate antiporter, system x_c^-, is essential for the efficient uptake of cystine into cells. Interest in the mechanisms of system x_c^- function soared with the recognition that system x_c^- presents the most upstream node of ferroptosis, a recently described form of regulated necrosis relevant for degenerative diseases and cancer. Since targeting system x_c^- hold the great potential to efficiently combat tumor growth and metastasis of certain tumors, we disrupted the substrate-specific subunit of system x_c^-, xCT (SLC7A11) in the highly metastatic mouse B16F10 melanoma cell line and assessed the impact on tumor growth and metastasis. Subcutaneous injection of tumor cells into the syngeneic B16F10 mouse melanoma model uncovered a marked decrease in the tumor-forming ability and growth of KO cells compared to control cell lines. Strikingly, the metastatic potential of KO cells was markedly reduced as shown in several in vivo models of experimental and spontaneous metastasis. Accordingly, survival rates of KO tumor-bearing mice were significantly prolonged in contrast to those transplanted with control cells. Analyzing the in vitro ability of KO and control B16F10 cells in terms

Abbreviations: CRISPR/Cas9, Clustered Regularly Interspaced Short Palindromic Repeats (CRISPR) associated protein 9 (Cas9); DEM, diethyl maleate; ER, endoplasmic reticulum; GSH, glutathione; Lip-1, liproxstatin-1; 2-ME, 2-mercaptoethanol.

of endothelial cell adhesion and spheroid formation revealed that xCT expression indeed plays an important role during metastasis. Hence, system x_c^- emerges to be essential for tumor metastasis in mice, thus qualifying as a highly attractive anticancer drug target, particularly in light of its dispensable role for normal life in mice.

KEYWORDS

melanoma, metastasis, system x_c^-, tumor growth

1 | INTRODUCTION

The cystine/glutamate transporter, system x_c^-, is a heterodimeric amino acid transporter consisting of the substrate-specific subunit, xCT (SLC7A11) and the 4F2 heavy chain (SLC3A2), a subunit shared by several other amino acid transporters.[1,2] System x_c^- exchanges extracellular cystine (or cystathionine) with intracellular glutamate at an equimolar ratio.[3,4] Cystine transported into cells is rapidly converted to cysteine and used for protein or glutathione (GSH) biosynthesis, the latter being the most abundant intracellular antioxidant in mammalian cells. Research into the biology of xCT has regained momentum with the discovery that system x_c^- is the most upstream player of ferroptosis. Ferroptosis is an iron-dependent form of necrotic cell death marked by an overwhelming phospholipid peroxidation,[5,6] and which emerges to be highly relevant for both degenerative diseases and cancer.[7] xCT expression and stability is known to be under the strict control of a number of cell-intrinsic and cell-extrinsic mechanisms. For instance, xCT is readily induced by oxidative stress and amino acid deprivation in a nuclear factor erythroid 2-related factor 2 (NRF2)- or activating transcription factor 4 (ATF4)-dependent manner, respectively. Accumulating evidence suggests that xCT expression is also under the control of the tumor suppressors p53 and BRCA1 associated protein 1 (BAP1), thus impacting on the cell's sensitivity towards ferroptosis.[8-10]

Metastasis is the leading cause of mortality in cancer, therefore prevention of cancer metastasis represents one of the central goals to substantially improve prognosis and quality of life for affected patients. As such, sulfasalazine treatment of nude mice bearing the human esophageal squamous cell carcinoma cell line KYSE150 markedly inhibited experimental lung metastasis indicating that system x_c^- could be involved in metastasis.[11] Moreover, vaccination of a virus-like particle presenting one of the extracellular domains of human/mouse xCT decreased the number of lung metastases in host mice implanted with murine lung cancer cell line.[12]

To provide unequivocal evidence of the relevance of xCT in cancer metastasis, we engineered the highly metastatic B16F10 mouse melanoma cell line to generate cells deficient in system x_c^-. Using cell-based studies as well as in vivo murine cancer models, we now demonstrate that xCT plays an essential role during various steps of metastasis in mice, while its targeted knockout ultimately increased survival rates of tumor-bearing mice. In light of the dispensable role of xCT for mouse embryogenesis and viability in mice,[13] our data strongly suggest that targeting system x_c^- is a highly promising approach to combat melanoma metastasis.

What's new?

The cystine/glutamate antiporter system xc- has generated growing interest as the most upstream node of ferroptosis, a recently-described iron-dependent form of necrotic cell death that is highly relevant in cancer. Using mouse cell-based assays and in vivo murine cancer models, here the authors demonstrate that system xc-deficiency not only impairs primary tumor growth but also abrogates tumor dissemination and metastasis in melanoma. The results also show in tumor-bearing mice that reduced metastasis coincides with increased overall survival. Overall, the findings support the essential role of system xc- in tumor metastasis and its potential as an attractive anti-cancer drug target.

2 | MATERIALS AND METHODS

2.1 | Chemicals

The following chemicals were purchased for the experiments: Lip-1 (Selleck Chemicals) and Z-VAD-FMK (Enzo Life Science). All other chemicals were obtained from Wako Pure Chemical Industries, Ltd. (Osaka, Japan), unless stated otherwise.

2.2 | Cell culture

B16F10 (CVCL_0159) was obtained from Cell Bank, RIKEN Bio-Resource Research Center (Ibaraki, Japan). xCT KO cells were generated from the parental cell line (WT), and R1, R2, R3 cell clones were established using xCT KO following methods described below. All B16F10 relevant cell lines were cultured routinely in RPMI1640 medium (Gibco) supplemented with 10% fetal bovine serum, penicillin (50 U/mL) and streptomycin (50 μg/mL). KO cells were maintained in medium supplemented with 2-ME (50 μM). Mouse embryonic fibroblasts (MEF) were established in a previous study[13] and cultured in DMEM supplemented with 10% fetal bovine serum, penicillin (50 U/mL) and streptomycin (50 μg/mL). The origin and characteristics of mouse lung endothelial cells (LE-1) have been described[14] previously and were kindly provided by Dr. Garth L. Nicolson. LE-1

were cultured in a mixture of F12 and DMEM (Nissui Pharmaceuticals) supplemented with 10% fetal bovine serum, penicillin (50 U/mL) and streptomycin (50 μg/mL). All cells were cultured at 37°C in 5% CO_2 and 95% air. All experiments were performed with mycoplasma-free cells.

2.3 | Generation of *xCT* KO and *xCT* reconstituted cells

xCT KO cells were generated by Clustered Regularly Interspaced Short Palindromic Repeats (CRISPR) associated protein 9 (Cas9) system-based technology. The guide RNA against *xCT* was designed by targeting the first exon (sequences: 5′-CTCCAGAACACGGGC AGCG-3′) and ligated into GeneArt CRISPR Nuclease Vector (Life Technologies, Carlsbad, California). The vector was transfected in B16F10 cells in the presence of 2-ME (50 μM). After 48 hours incubation, the transfected cells were trypsinized and 100 cells were plated on 100 mm-diameter dishes to allow formation of independent colonies. Single-cell colonies were picked and transferred into 96 well plates, splitted and then plated into two wells and cultured in the presence or absence of 2-ME. Cells knockout (KO) for the xCT gene would die in the absence of 2-ME, while the cells with 2-ME would proliferate. One single-cell clone which satisfied these criteria was obtained, and Western blot analysis confirmed the KO of xCT. To re-express xCT in KO cells, the xCT expression plasmid pEF-BOS[15] kindly provided by Kazuichi Sakamoto (University of Tsukuba, Ibaraki, Japan) was transfected into KO cells in the presence of 2-ME. Then, 48 hours after transfection, xCT expressing cells were obtained by culturing in 2-ME-free medium. The functional restoration of xCT of the isolated clones (R1, R2 and R3) was confirmed by cystine transport activity, immunoblot analysis and total glutathione levels.

2.4 | Measurement of amino acid transport activities

Uptake of arginine, cystine, leucine and serine in WT cells and KO cells was measured as described previously.[16]

2.5 | Determination of total intracellular glutathione

Intracellular total (reduced and oxidized) glutathione concentrations were measured by the enzymatic method as described.[16]

2.6 | Measurement of extracellular cysteine

Extracellular cysteine levels from cell culture supernatant were measured following as reported previously.[13]

2.7 | Western blotting

SDS-PAGE and Western blotting were performed according to previous reports.[17] Mouse xCT was detected using a specific monoclonal antibody. In brief, a monoclonal antibody against mouse xCT (clone 4B3, rat IgG2b) was generated by immunization of Lou/c rats with ovalbumin-coupled peptide GRLPSMGDQEPPGQE using standard procedures.[18] β-actin (Sigma-Aldrich, St. Louis, Missouri, #A5441) was detected as an internal control. Further information can be found in the Supporting Information Materials and Methods.

2.8 | Determination of cell number

Cell number was measured by the trypan blue exclusion method as described.[16]

2.9 | Assessment of lipid peroxidation

Cells were plated into six-well plates (10×10^4 cells/well) in the presence of 2-ME (50 μM). Three hours after incubation, 2-ME was washed out by prewarmed PBS and PBS was replaced by fresh RPMI medium containing either 2-ME (50 μM) or Lip-1 (500 nM). Then, cells were kept in culture for another 48 hours. After this treatment, lipid peroxidation in these cells was assessed as reported previously[19] using a flow cytometer (FACS Canto II, BD Biosciences, San Jose, California).

2.10 | Cell cycle stage analysis

Cells were plated in six-well plates (5×10^4 cells/well) and cultured for 48 hours in the presence of 2-ME (50 μM). Following the incubation, cells were washed with prewarmed PBS, and fresh RPMI medium containing either 2-ME (50 μM), or Lip-1 (500 nM), or Z-VAD-FMK (50 μM) was added, and kept in cell culture for another 24 hours. DNA staining was performed using propidium iodide-based DNA staining kit (Beckman Coulter, Brea, California, #C03551) according to manufacturer's instructions. After staining, PI fluorescence was detected using 488 nm laser for excitation using a flow cytometer (FACS Canto II, BD Biosciences).

2.11 | Spheroid formation and ATP measurements

Cells were seeded at 2×10^4 cell/200 μL of medium in U-shaped bottom 96-well plates to allow them to grow scaffold-independent and to form spheroids. After 72 hours, spheroids were collected in tubes with 50 μL of medium. Then, 50 μL of Cell Titer-Glo 3D reagent (Promega) were added and the ATP level was measured in a spheroid following the manufacturer's instructions. Further information can be found in the Supporting Information Materials and Methods.

2.12 | Tumor cell-endothelial cell adhesion assay

The tumor cell adhesion assay was performed according to a previously reported method.[20]

2.13 | Cell migration

Cell migration was evaluated by scratch assay based on the method of Liang with minor modifications.[21] Cells were seeded at 2.0×10^5 cells/well of a 12-well plate and cultured for 24 hours to yield a confluent monolayer. Then, a linear wound was made with a sterilized 200 μL pipette tip. Cells were washed twice with serum-free medium and 2 mL of fresh serum-free medium were added. Pictures were taken at different time points and the extent of migration was quantified by ImageJ (U. S. National Institutes of Health, Bethesda, Maryland, https://imagej.nih.gov/ij/, 1997-2016).

2.14 | Cell invasion

Cell invasion was assessed using the Transwell (Corning) invasion assay (Boyden chamber assay). One day prior to this assay, 5×10^4 of MEF were seeded on a 24-well plate and cultured for 24 hours. On the following day, Matrigel (Corning, New York) was diluted and coated on Falcon cell culture insert transparent PET membrane with 8.0 μm pore (Corning) following manufacturer's instructions and incubated at 37°C for 2 hours. B16F10 cell lines were re-suspended in serum-free medium at 5×10^4 cells/mL. Finally, each cell suspension was added into the Matrigel coated-insert, and the insert was set in the 24 well plate with MEF cells. After 12 hours of incubation, the inserts were fixed with 100% ethanol and stained with Mayer's hematoxylin and 1% Eosin Y Solution. Noninvaded cells on the inside of inserts were removed by cotton swab. Invaded cells on the outside of inserts were counted using ImageJ.

2.15 | Animal experiments

Female C57BL/6 mice (5 weeks old) obtained from Nippon SLC (Hamamatsu, Japan) were maintained under specific-pathogen-free conditions with light from 7:00 AM to 7:00 PM, at 23 ± 3°C and 50 ± 10% humidity in the Institute for Animal Experimentation Tottori University and used after 1-week acclimatization. Diet and water were supplied and consumed ad libitum throughout the experiments. All surgical and euthanasia procedures were performed under inhaled isoflurane (095-06573, Wako Pure Chemical, Osaka, Japan) anesthesia. At the end of the in vivo tumor experiments, mice were sacrificed and dissected when they either became moribund state or reached a given time point for evaluating the tumors' malignancy.

2.16 | In vivo tumor growth

Cells were suspended in serum-free DMEM. Then, 2×10^6 cells in a 200 μL were implanted subcutaneously into the right flank of mice, and then tumor size was measured using calipers.

2.17 | Experimental metastasis model

For intravenous injection, 1×10^5 cells in a 200 μL were injected into mice via tail vein. For intrasplenic injection, 1×10^6 cells in a 10 μL of the serum-free medium were injected into the spleen of anesthetized mouse. A few minutes later, the spleen was removed to prevent primary tumor formation in the spleen.

2.18 | Experimental dissemination (intraperitoneal injection)

To examine peritoneal dissemination, 5×10^5 tumor cells in a 500 μL was injected into the peritoneal cavity.

2.19 | Spontaneous metastasis (intra-footpad injection)

Next, 5×10^5 of tumor cells in a 25 μL were injected into the right footpad of mice. When the primarily growing tumors reached over 100 mm^3 in volume, the leg containing the tumor was amputated.

2.20 | Statistical analysis

Data obtained from in vitro experiments were analyzed using GraphPad Prism8 (GraphPad Software, La Jolla, California). Student's *t*-test or One-way or Two-way ANOVA followed by Tukey's multiple composition test were performed using the software. Data from animal experiments were analyzed using the same software and Log-rank test was performed for assessing the significance in each survival curve from different tumor-bearing mice.

3 | RESULTS

3.1 | Generation and characterization of *xCT*-deficient melanoma cells

To explore in detail the role of xCT in cell-based and in vivo models of tumor metastasis, we focused on the mouse melanoma cell line, B16F10, which was originally established by in vivo selection owing to their growth potential and their ability to form distant metastasis in various organs.[22] First, B16F10 cells were transfected with CRISPR/Cas9

system targeting exon 1 of the *xCT* gene and then kept in medium containing 2-mercaptoethanol (2-ME; Figure 1A). 2-ME reacts with cystine to generate cysteine and cysteine-2-ME mixed-disulfide, both of which are taken up by neutral amino acid transporters, thereby bypassing the need for system x_c^-.[23] One hundred single-cell colonies were isolated and cultured individually. Upon reaching confluency, cells were divided into two wells containing medium with or without 2-ME, allowing for the selection of single-cell clones that do not survive in the absence of 2-ME due to cysteine starvation and massive GSH depletion (Figure 1A).

Matched clones were selected and immunoblot analysis confirmed that xCT expression was abolished in the KO clone (Figure 1B). Furthermore, measurement of cystine transport activity showed no detectable activity in KO cells compared to parental B16F10 (WT) cells (Figure 1C), corroborated by the concomitant loss of intracellular GSH (Figure 1D). Diethyl maleate (DEM), an electrophile and potent inducer

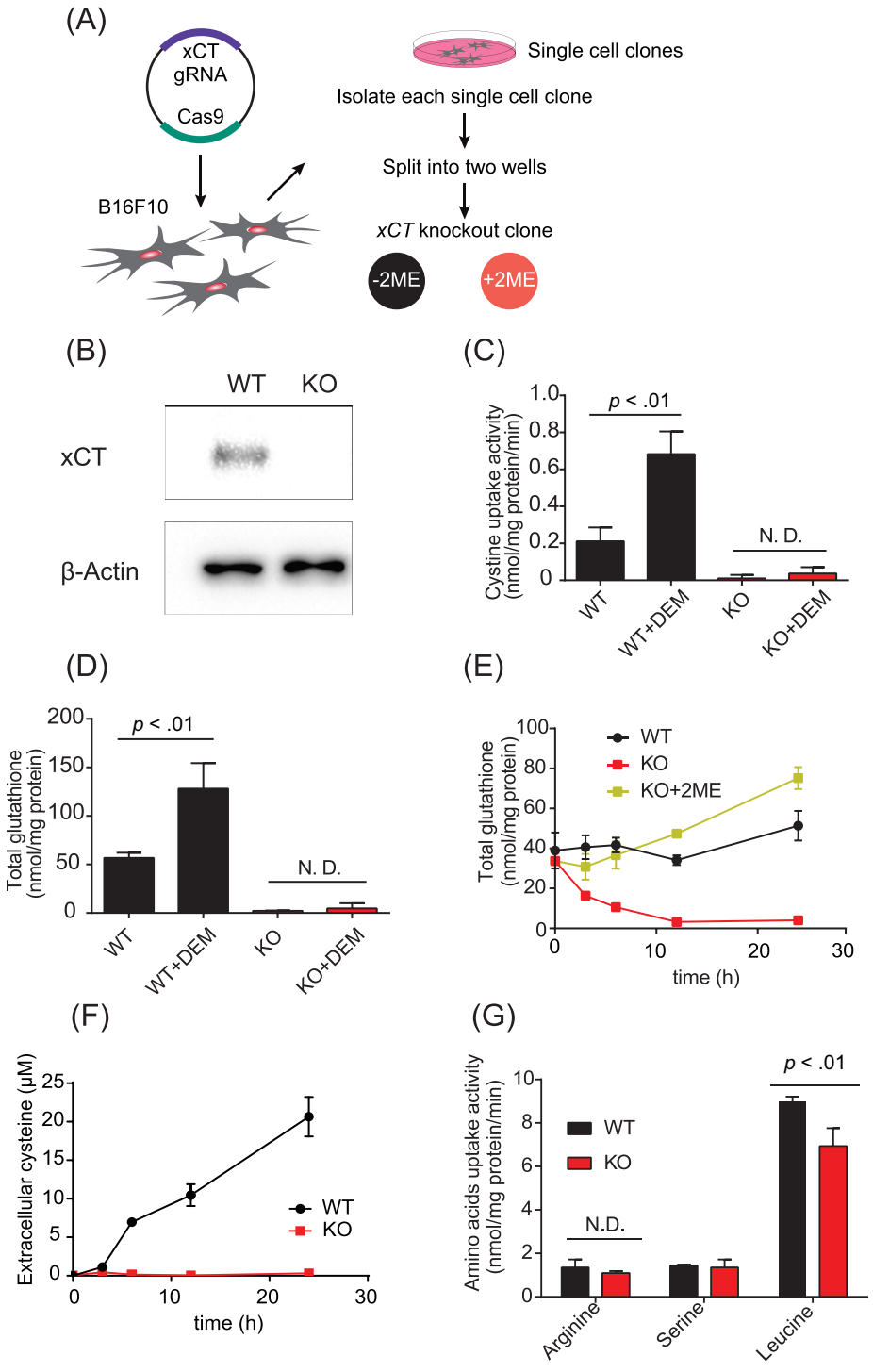

FIGURE 1 Generation of *xCT* knockout B16F10 cells. A, A brief schematic overview of generating *xCT* knockout (KO) clones. B, xCT level in WT and KO cells was determined by immunoblotting. C, Cystine uptake activity in WT and KO cells with DEM simulation. Cells (2×10^5) were seeded and 100 μM of DEM was added to cells 12 hours before the measurement. D, Intracellular total (reduced and oxidized) glutathione levels in WT and KO cells exposed to DEM. Cells (2×10^5) were seeded and 24 hours before sampling, 100 μM of DEM was added to cells. E, Time course of glutathione levels in WT and KO cells. Cells (2×10^5) were seeded and incubated for 24 hours. Then, cells were washed with PBS and replaced fresh medium in the absence or presence of 50 μM 2ME (0 hour) and incubated for another 24 hours. F, Extracellular cysteine levels of WT and KO cells were determined by HPLC **g** Amino acid uptake activity in WT and KO cells was measured using [^{14}C] labeled amino acids. Data (B-E) are presented as mean ± SD, n = 4 (B, E, G), n = 4-5 (C), n = 2 (D). *P* values were obtained by Student's *t*-test between WT and WT + DEM or KO and KO + DEM (C and D). N.D. means no significant difference

of xCT,[24] had no effect on cystine uptake activity and intracellular GSH levels in KO cells in contrast to WT cells (Figure 1C, D). Figure 1E illustrates the change of intracellular GSH in WT and KO cells with or without 2-ME. According to our previous data,[25] accumulation of extracellular cysteine was observed only in the medium of WT cells, but not of KO cells (Figure 1F). From these data, it can be concluded that *xCT* KO B16F10 cells are devoid of any detectable system x_c^- activity.

Next, we determined the activities of other amino acid transport systems, such as arginine, serine and leucine, which are typical substrates of systems y+, ASC and L, respectively. No difference was observed with respect to the activities of systems y+ and ASC, whereas leucine uptake was modestly decreased in KO compared to WT cells (Figure 1G). Since 4F2 heavy chain (SLC3A2) is conserved among amino acid transporters and a common component of systems

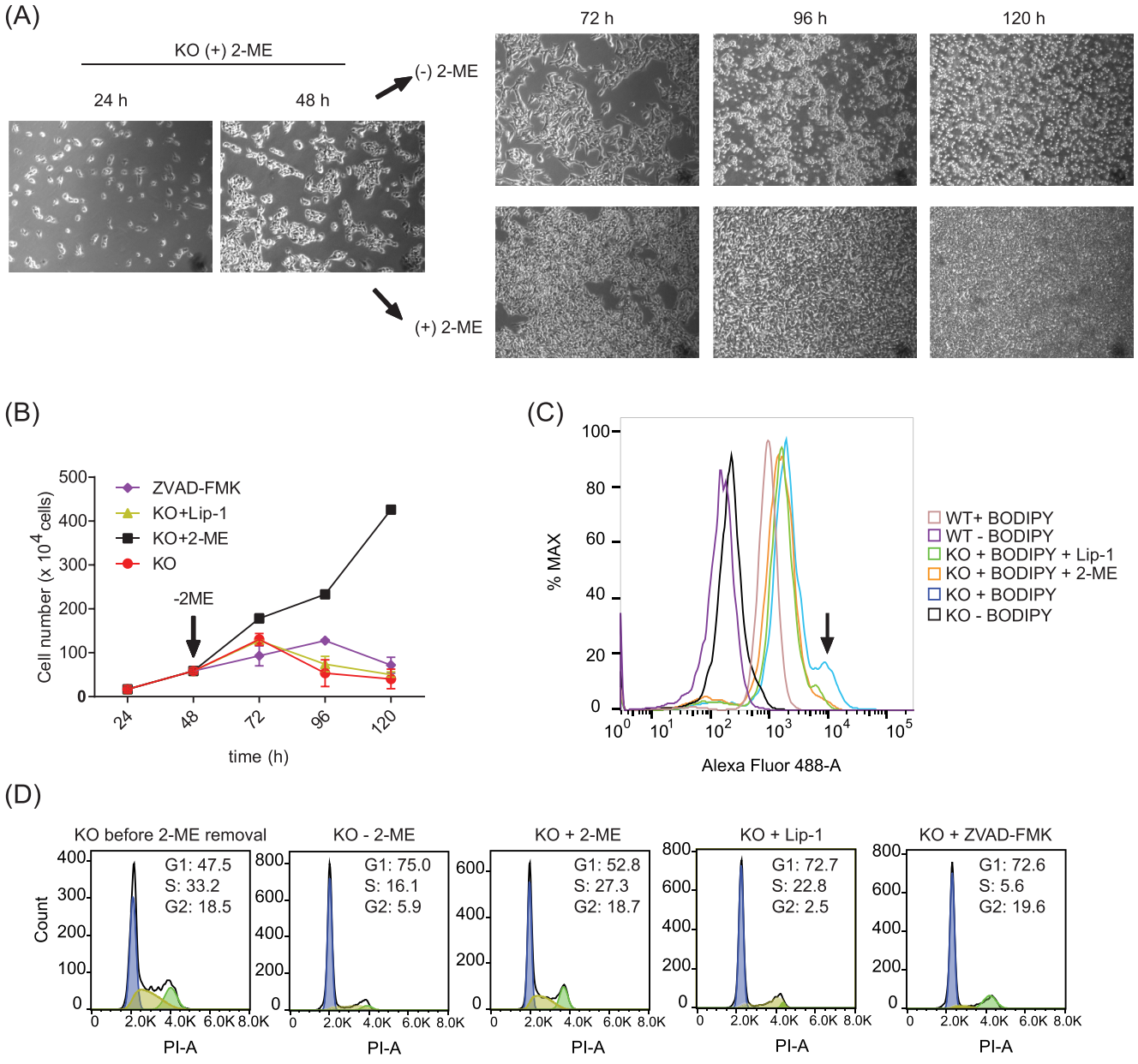

FIGURE 2 Characterization of KO cells in cell growth. A, Pictures of xCT-KO cells in the presence or absence of 2-ME (50 μM) are shown. Then, 10×10^4 KO cells were cultured for 48 hours with 2-ME. Then, cells were washed with PBS, and fresh RPMI medium supplemented with 2-ME or with distilled water as control was added to be cultured for another 72 hours. B, Cell growth curves were obtained by trypan-blue exclusion method. Then, 10×10^4 of KO cells were initially plated in the presence of 2-ME (50 μM) and cultured for 48 hours. Subsequently, cells were washed with PBS, and continued culture in fresh medium containing either 2-ME (50 μM), Lip-1 (500 nM) or ZVAD-FMK (50 μM). C, Assessment of lipid peroxidation by BODIPY581/591 C11 using flow cytometry. The arrow points at the fluorescence shift induced by lipid peroxidation. D, Cell cycle analysis was performed by propidium iodide-based DNA staining and flow cytometry. The numbers beside the graphs demonstrate the percentage of each cell cycle phase. Data in B are presented as mean ± SD, n = 2. C and D are shown one representative experiment in three (B) and two (D) independent assay

x_c^- and L, disruption of xCT may thus affect the activity of leucine transport in KO cells, at least to some extent.

xCT KO cells failed to proliferate over time in the absence of 2-ME, whereas 2-ME supplementation restored normal cell growth. Moreover, KO cells started dying 48 hours after 2-ME removal, and after another 24 hours, living cells were hardly detectable. (Figure 2A, B). Previously, it was shown that pharmacological inhibition of xCT by the small molecule erastin results in GSH depletion, increased lipid peroxidation and ultimately cell death by ferroptosis.[5,26,27] Therefore, we asked whether treatment with the ferroptosis inhibitor liproxstatin-1 (Lip-1) would compensate for the loss of xCT in B16F10 cells. Surprisingly, Lip-1 failed to rescue cell proliferation, unlike 2-ME supplementation (Figure 2B), albeit preventing lipid peroxidation (Figure 2C). Likewise, ZVAD-FMK, a pan-caspase inhibitor, failed to restore cell growth in xCT KO cells. To study potential effects of xCT depletion on cell cycle progression, we next assessed cellular DNA content. Indeed, 2-ME withdrawal from KO cells resulted in an impaired cell cycle, as evidenced by decreased percentage of cells in the S and G2/M phase, which, however, could not be rescued by Lip-1 or Z-VAD-FMK (Figure 2D). Analysis of endoplasmic reticulum (ER) stress revealed expression of the ER chaperone GRP78/BiP revealed increased ER stress in xCT KO cells deprived of 2-ME

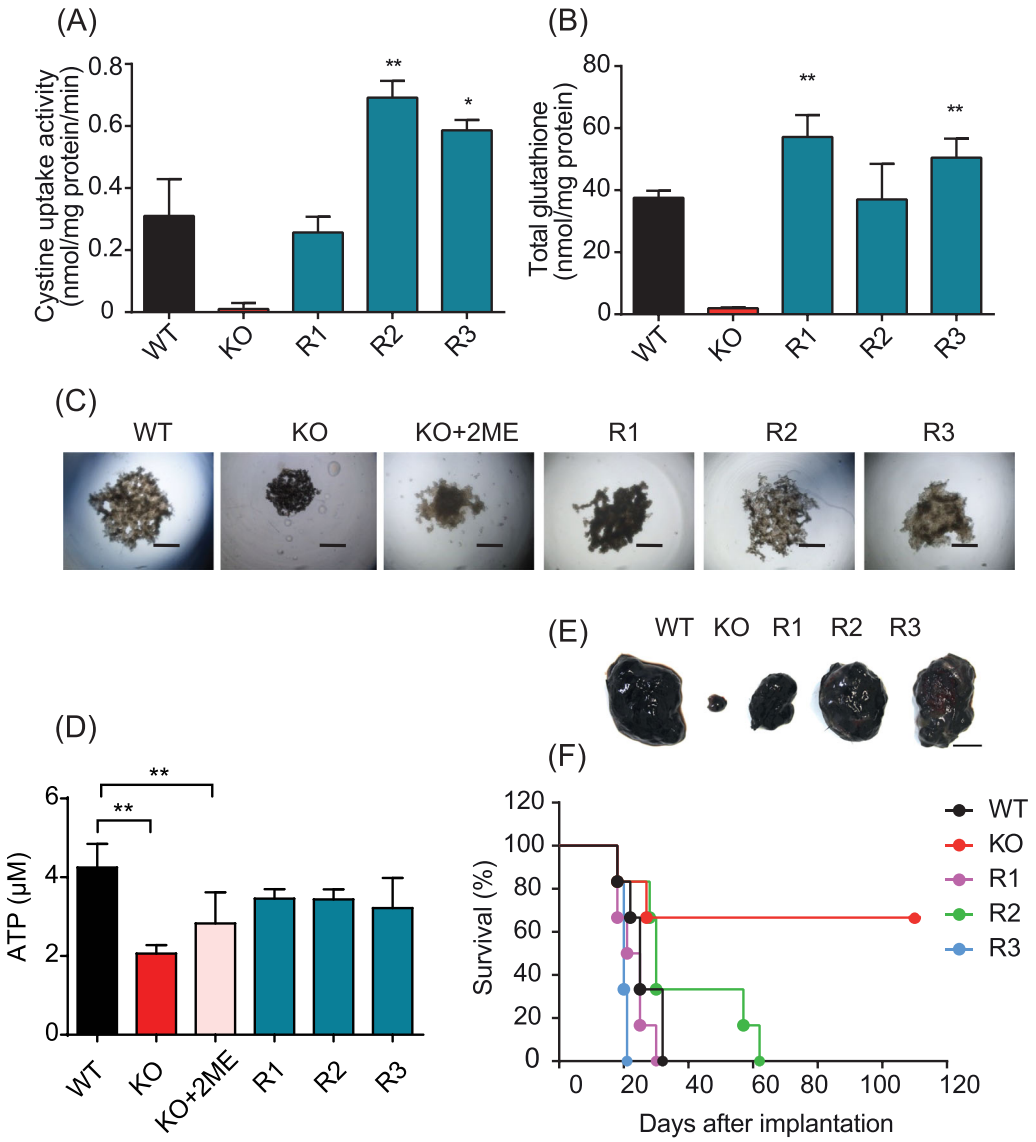

FIGURE 3 Impaired tumorigenicity of KO cells in spheroid forming assay and subcutaneous tumor transplantation. A, Cystine uptake activity was measured in WT, KO and xCT gene-addback clones (R1, R2 and R3) using [^{14}C] labeled cystine. B, Intracellular total glutathione level was measured in WT, KO and R1-R3 cells. C, Representative pictures of spheroids derived from WT, KO and R1-3 cells 72 hours after culturing in a U-shaped bottom 96-well. The scale bars show 0.5 mm. D, ATP level in the spheroids corresponding to (C). E, A representative picture of tumors dissected 18 days after the subcutaneous transplantation of 2×10^6 cells into syngeneic (C57BL/6) mice. The scale bar shows 10 mm. F, Kaplan-Meier curves were obtained from all the six mice transplanted with each cell line. A, B and D are presented as mean ± SD, n = 4. *P* values were obtained using one-way ANOVA followed by Tukey's multiple comparison test (*$P < .05$, **$P < .01$ vs WT)

(Figure S1), which is in line with earlier data showing that inhibition of system x_c^- causes ER stress.[28] Analogous to the expression pattern of GRP78 we also found increased levels of the autophagosome marker LC3 (Figure S1), however, neither ER stress nor the enhanced levels of LC3 could be abrogated by Lip-1 in contrast to 2-ME (Figure S1).

3.2 | xCT deficiency impairs spheroid formation ability and primary tumor growth but prolongs survival of tumor-bearing mice

To reconstitute xCT expression, KO cells were transfected with an *xCT* expression plasmid and selected by depriving cells of 2-ME. Three independent clones (R1, R2 and R3) were selected and analyzed in terms of cystine transport activity and intracellular GSH levels. As shown in Figure 3A,B, cystine transport activity was equivalent (R1) or even higher (R2 and R3), and intracellular GSH was equivalent (R2) or even higher (R1 and R3), as compared to those of WT cells. Higher cystine transport activity and GSH levels in some clones may arise from the insertion of the xCT expression vectors with different copy numbers into random positions of the genome of xCT KO cells. For studying spheroid formation, we cultured the different cell lines in U-shape wells for 72 hours before cell viability was determined by ATP measurement. As illustrated in Figure 3C,D, ATP levels as well as the spheroid size of KO cells were reduced by approximately half, compared to WT, while ATP levels were restored in R1-3 cells to

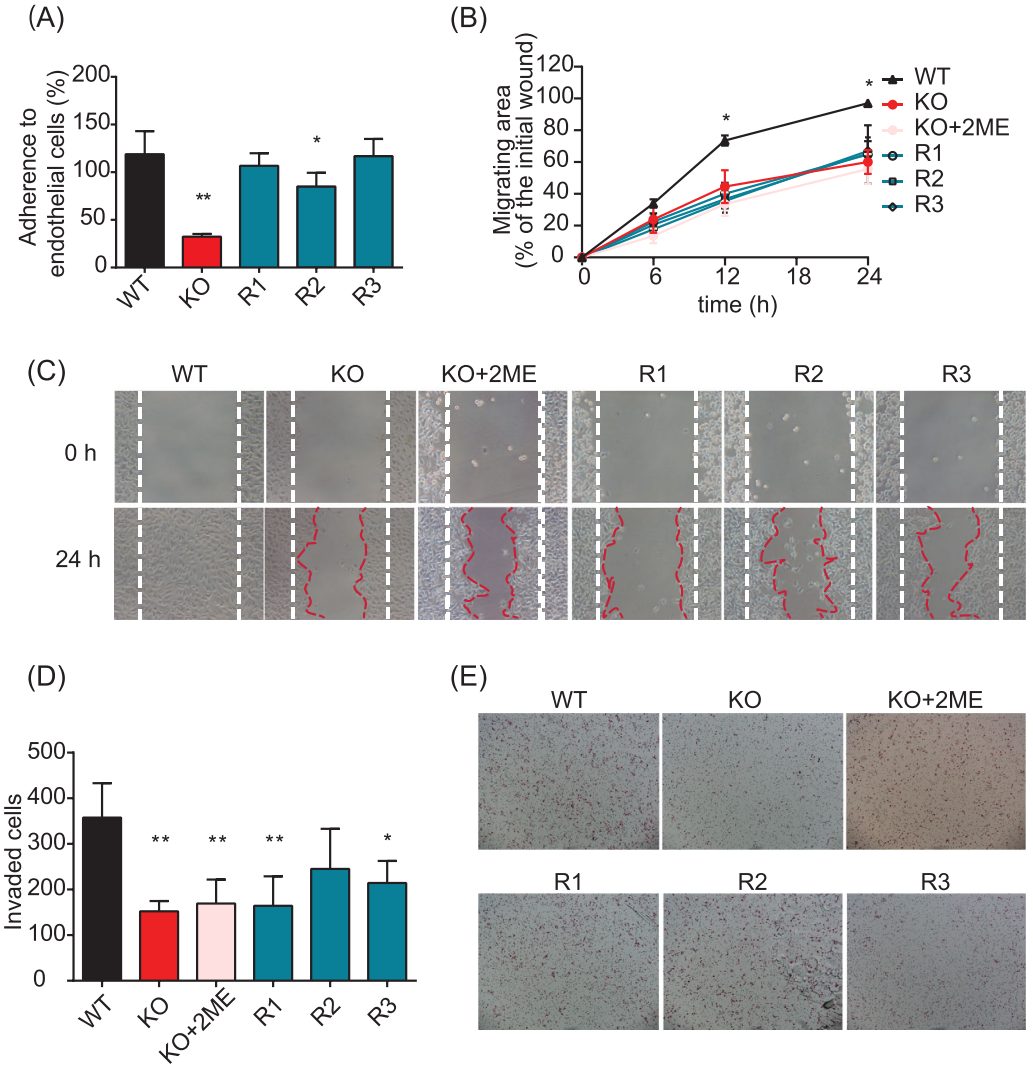

FIGURE 4 xCT contributes to various processes in *in vitro* tumor metastasis models. A, Cell-to-cell adherence capability of WT, KO R1-3 cells is shown as percentage of these cells adhering to endothelial cells (LE-1). B, Cell migration rate (% of initial wound area) was calculated using ImageJ software. C, Representative pictures of cell migration at the beginning of this assay and its endpoint (24 hours) are shown. The white-broken lines indicate the edge of cell monolayer after scratching cell surface by a sterilized P200 tip. The red-broken lines indicate the edge of the cell monolayer after migration into the open space. D, The number of invaded cells from *in vitro* invasion assay using Matrigel and transwell. Invaded cells were stained with hematoxylin and eosin solution and counted using ImageJ software. Data are presented as mean ± SD, n = 5 (A), n = 4 (B), n = 4-6 (D). *P* values were obtained using one-way and two-way (time point × treatment in B) ANOVA followed by Tukey's multiple comparison test (*$P < .05$, **$P < .01$ vs WT)

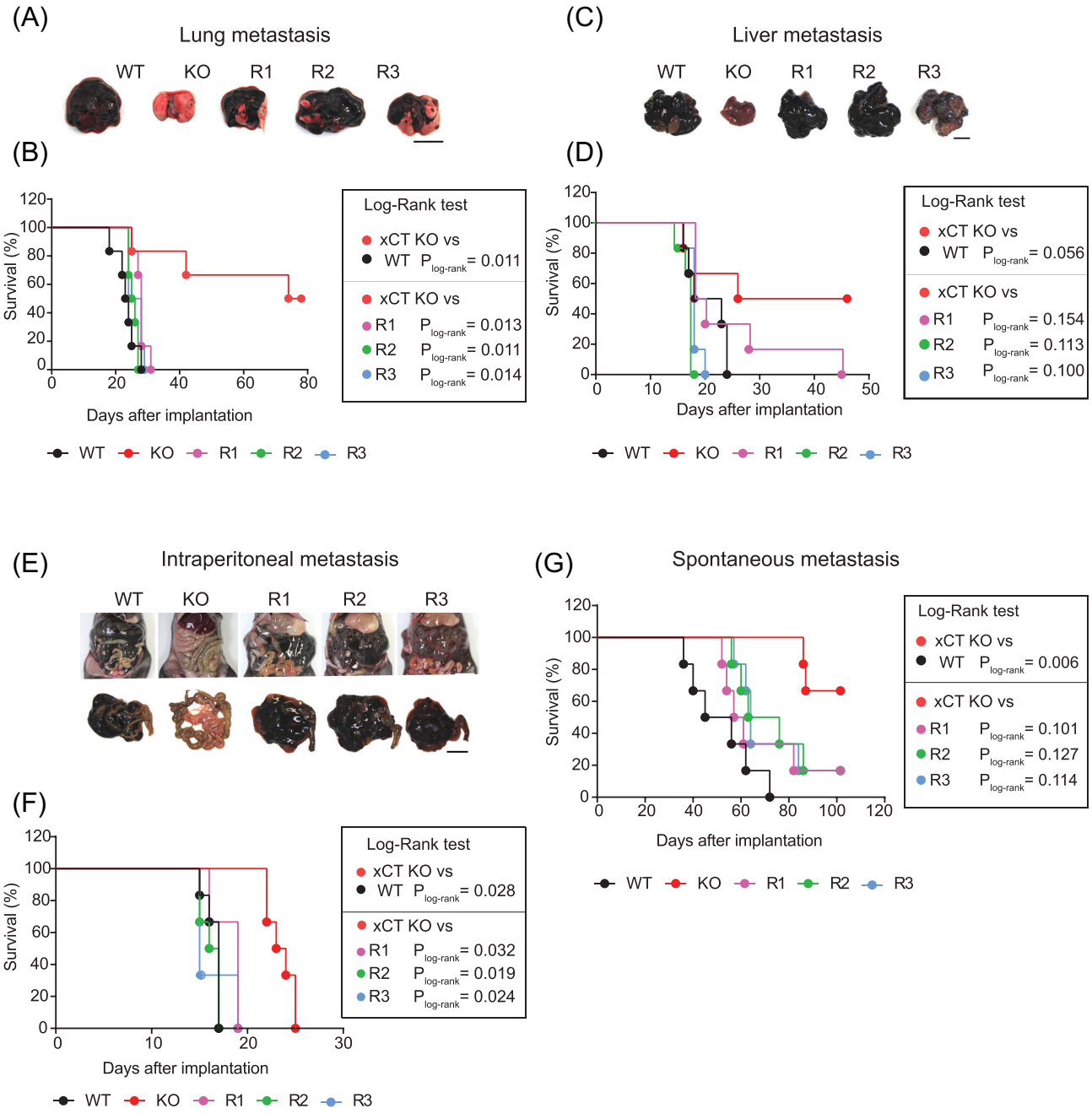

FIGURE 5 Experimental metastasis is suppressed in xCT-deficient tumors associated with considerably increased survival rates. A, Lung metastasis model: Representative pictures of lung with tumor isolated 28 days after the transplantation of 1×10^5 cells injected into tail vein of mice as an experimental model for lung metastasis. The scale bar indicates 10 mm. B, Survival curves were obtained by the Kaplan-Meier's method from all six mice transplanted with each cell line. C, Liver metastasis model: Representative pictures of liver with tumor dissected at 16 days after the injection of 1×10^6 cells into spleen of mice followed by the resection of the spleen 5 minutes after tumor cell inoculation, as an experimental model for liver metastasis. The scale bar shows 10 mm. D, Survival curves were obtained by the Kaplan-Meier's method from all six mice transplanted with each cell line. e Disseminated metastasis to the peritoneal cavity: 5×10^5 cells each were intraperitoneally injected into mice as an experimental model for disseminated metastasis. Representative pictures of tumor formation in peritoneal cavity and omentum 16 days after the transplantation are given (scale bar indicates 10 mm). F, Kaplan-Meier's curves were obtained using all six mice transplanted with each cell line. G, Spontaneous metastasis model: 5×10^5 cells each were transplanted into the footpad of mice. Upon primary tumor formation, lung metastasis was examined after the primary tumor reached a size of 100 mm^3. Survival curves were obtained by the Kaplan-Meier's method from all six mice transplanted with each cell line. In all panels, the significance of data was assessed by the Log-rank test

levels that seen in WT cells. KO cells in the presence of 2-ME showed a trend of higher ATP levels, compared to KO alone, yet the ATP levels were not significantly different from those of R1-3 cells. These results suggest that spheroid formation is dependent on intracellular GSH level. Moreover, we evaluated the number of spheroids with more than 40 μm diameter in WT, KO and R1-3 cells as alternative

method and observed a significantly lower number of spheroids in KO cells as compared to control cells (Figure S2A,B).

To examine the role of xCT in tumor formation, we injected WT, KO and R1-3 syngeneic B16F10 melanoma cells subcutaneously into C57BL/6 mice. Tumor growth was comparable in tumor diameter and weight between WT and reconstituted cell lines (R2 and R3) until mice had to be sacrificed due to humane endpoint (Figure 3E, Table S1). Although the tumor diameter of R1 seems to be smaller than that of WT, it was still significantly bigger than that of KO. Importantly, a significant prolongation of latent period and the period when the tumor mass reached 10 mm in a diameter was observed in the KO compared to control cell lines (Table S1; $P < .01$). Subcutaneous tumor size and weight at the time of autopsy were also markedly reduced in KO cells compared to WT or R1-3 cells (Figure S3 and Table S1; $P < .05$). Remarkably, the overall survival of tumor-bearing mice was robustly prolonged in KO as compared to WT or R1-3 tumor-bearing mice (Figure 3F).

3.3 | xCT contributes to various processes in in vitro tumor metastasis models

Next, we asked whether xCT plays a pivotal role in certain steps contributing to melanoma metastasis. We performed in vitro studies reflecting key processes in the metastatic cascade. We first analyzed adhesion to endothelial cells as an initial critical step in the formation of blood-borne metastasis, according to our previously established in vitro assay.[29] As shown in Figure 4A, attachment of KO cells to mouse lung endothelial cells was significantly lower than in WT and R1-3 cells ($P < .01$), suggesting a potential contribution of xCT in adhesion processes to vascular endothelium.

To determine the migration potential of WT, KO and R1-3 cells, in vitro scratch assays were performed. The wounded area was nearly full of migrated WT cells after 24 hours, whereas only approximately 50% was occupied by KO cells (Figure 4B and Figure 4C). Unexpectedly, the migration activity of KO cells could not be rescued by 2-ME or in the reconstituted cells (R1-3). Finally, we determined the invasion ability of xCT KO and control cells using the transwell invasion assay. As shown in Figure 4D,E, the number of invaded KO cells was less than half of that in WT cells, and also the number of invaded R1 and R3 cells was significantly lower than that of WT cells. In addition, even when KO cells were plated in the upper well in the presence of 2-ME, invaded cells were still significantly lower than that of WT cells.

3.4 | Experimental and spontaneous metastasis is suppressed in *xCT* KO B16F10 melanoma cells in vivo

Due to the inherently stark differences in the redox conditions between cell culture and whole organisms,[13] we then focused on in vivo metastasis models. To determine the experimental metastatic ability of the cell lines in colonizing lungs, WT, KO and R1-3 cells were first injected into the tail vein of mice. In the absence of xCT, B16F10 KO cells failed to form lung metastases, whereas WT and R1-3 cells formed lung colonies to slightly varying degrees (Figure 5A, Table S2). Since weight measurement reflects an increase in metastatic nodules, lungs resected from KO animals weighed less compared to WT or R1-3 cell-injected mice (Table S2). R1-3 cells yielded similar lung colonizing ability and weights as WT cells (Table S2). Moreover, survival rates of mice were significantly prolonged in the KO cell group compared to WT or R1-3 tumor cells (Figure 5B, Table S2).

Next, we examined the metastatic ability of B16F10 cells to colonize the liver, whereupon WT, KO and R1-3 cells were injected intrasplenically. We observed a clearly reduced metastatic potential of KO tumor cells (Figure 5C, Table S3). The mean survival days of tumor-bearing mice was prolonged in animals receiving KO cells compared to the other groups (Figure 5D). Moreover, the mean liver weight, which reflected metastatic nodules formed in the liver, was lower in KO tumor cells than in mice injected with WT or R1-3 cells; yet it failed to reach statistical significance.

When mice were intraperitoneally injected with WT, KO and R1-3 cells, all of the mice formed tumors in the peritoneal cavities. However, a decreased aggressiveness was observed in KO cell-injected mice compared to controls (Table S4). After 16 days of tumor inoculation, mice were euthanized and examined for tumor formation in the peritoneum and omentum (Figure 5E). KO cells were reduced or delayed in their ability to form tumors in the peritoneum including omentum leading to increased survival rate of mice (Figure 5F). Moreover, the frequency of peritonitis carcinomatosa formation and its related quantity of ascites was significantly suppressed in KO cells (Table S4). Therefore, the aggressiveness of tumor cells after peritoneal dissemination is strongly reduced in KO cells compared to WT and R1-3 cells.

Finally, we injected WT, KO and R1-3 tumor cells into the footpad of mice as an experimental model of spontaneous metastasis of tumor cells to distant organs. We observed that the latency period and the period when the tumor mass reached 100 mm^3 of volume, which means the capability of primary tumor growth, was significantly prolonged in mice injected with KO cells (Figure 5G, Figure S4 and Table S5). These results are consistent with primary tumor growth in the subcutaneous sites (Figure 3E and Table S1). The incidence and the number of lung nodules were significantly reduced and survival period was prolonged in the KO group (Tables S2 and S5). At the time of sacrifice, there was no evidence of visible spontaneous metastasis to distant organs except lungs.

4 | DISCUSSION

Using a well-defined model of the highly metastatic tumor cell line B16F10 genetically engineered to lack xCT, the substrate-specific subunit of system x_c^-, we now provide conclusive evidence that system x_c^- deficiency not only impairs primary tumor growth (Figure 3), but also abrogates tumor dissemination and metastasis in diverse syngeneic models of experimental and distant metastasis (Figure 5). We further found that strongly reduced metastasis coincides with markedly increased overall survival of tumor-bearing mice.

Our in vitro analyses further suggest that xCT may contribute to various aspects of tumor metastasis including the ability to form spheroids, adherence to endothelial cells, migratory activity and invasion ability. As shown in Figure 3, intracellular GSH maintained by xCT seems to be a crucial role for spheroid formation. However, migratory activity and invasion ability in KO cells treated with 2-ME and R1-3 cells did not recover to levels as seen in WT cells. These results suggest that intracellular GSH maintained by xCT is not involved in these in vitro migration and invasion models. Polewski et al reported that overexpression of xCT causes cytoskeletal changes as well as decreased migration and invasion in glioma cells.[30] It is noteworthy that in R1-3 cells expression of xCT cannot be controlled by extrinsic and/or intrinsic mechanisms which is different from wild-type cells that ultimately allow the dynamic induction of intrinsic *xCT* gene expression when required. As such, future studies are warranted to address whether carefully controlled xCT expression may have an impact on the individual steps of tumor metastasis in these in vitro models. Since in vivo metastasis is a multi-step process including epithelial-mesenchymal transition, invasion, intravasation, adherence and migration into distant organs, metastasizing tumor cells are known to undergo vigorous metabolic changes and to experience oxidative stress. It is well-accepted that xCT is strongly induced by various stimuli, including oxidative stress and amino acid deprivation.[31-34] It is thus conceivable that during the invasion-metastasis cascade[35] invaded tumor cells upregulate xCT in the blood and lymphatic vessels due to higher oxygen tensions in blood,[36] which probably plays a pivotal role for invaded tumor cells to transit through hematogenous and lymphatic systems. Only cells competent to induce the de novo expression of xCT by oxygen might be able to survive and reach their metastatic site.

In recent years, it is emerging that glutamate and its receptors play an important role in tumor development, acting as a growth factor and a signal mediator in tumor tissues.[37] Thus, it is highly likely that glutamate released by xCT is involved in some steps of metastasis such as tumor proliferation, invasion and migration via autocrine and/or paracrine mechanisms in vivo. Briggs et al demonstrated that increased extracellular glutamate released by triple-negative breast cancer cells inhibits cystine transport via xCT, leading to intracellular cysteine depletion.[38] Hypoxia-inducible factor (HIF) is a master transcription factor of genes that support adaptation to hypoxic conditions and this intracellular cysteine depletion inhibits the HIF1α prolyl-hydroxylases, resulting in HIF1α accumulation. Lu et al reported that chemotherapy induced the expression of xCT and the regulatory subunit of glutamate-cysteine ligase in a HIF-dependent manner, resulting in increased intracellular glutathione, which induced the breast cancer stem cell phenotype.[39] Thus, xCT indirectly regulates the expression of the genes that promote angiogenesis, erythropoiesis, glycolysis, autophagy and energy conservation through HIF1α.

Interestingly, although B16F10 xCT KO cells do not express system b^{0+}, another cystine transporter present in kidney, nor enzymes of the transsulfuration pathway (data not shown), they do survive for 24 and 48 hours after 2-ME removal, albeit were unable to proliferate; this is in stark contrast to fibroblasts lacking xCT which readily die upon 2-ME removal.[13] In addition, xCT KO cells displayed increased lipid peroxidation and cell cycle arrest, which could be rescued by 2-ME; however, the ferroptosis inhibitor Lip-1 can only rescue increased lipid peroxidation but not cell cycle arrest in xCT KO cells. Moreover, xCT reconstituted KO cells and other human melanoma cell lines can survive in cystine-free medium (data not shown). These phenomena may depend on the antioxidant properties of melanin.[40] A similar phenomenon was observed when xCT-deficient fibroblasts were cultured under routine culture conditions in the presence of vitamin E,[13] whereby the fibroblasts did not proliferate, but still survived for 48 hours under these conditions.

In conclusion, ours and others data reinforce the notion that targeting system x_c^- is a highly promising and valid anticancer approach. Nonetheless, in light of the essential role of xCT for tumor growth and in particular metastasis as well as the dispensable role for xCT in mouse survival,[13] T-cell proliferation and antitumor immunity,[41] it is mandatory to fully explore the pharmacological potential of efficient system x_c^- targeting using either highly potent small molecule compounds as stand-alone/combination therapies or immunotherapies.[16,28,42]

ACKNOWLEDGEMENTS

This work was supported by Japan Society for the Promotion of Science KAKENHI Grant Number JP17K07158 to H. S., the Deutsche Forschungsgemeinschaft (DFG) CO 291/5-2 and CO 291/7-1 and the m4 Award provided by the Bavarian Ministry of Economic Affairs, Regional Development and Energy (StMWi) to M. C., the Rudolf Virchow Center Jr group leader (University of Würzburg), the DFG (FR 3746/3-1) and the IZKF (B424) to J. P. F. A. and the Uehara Memorial Foundation Overseas postdoctoral fellowships to M. S.

CONFLICT OF INTEREST

The authors declare no competing interests.

ETHICS STATEMENT

In vivo experiments were performed in accordance with protocols approved by the Committee of the Institute for Animal Experimentation of Tottori University (16-Y-32).

DATA AVAILABILITY STATEMENT

The datasets that support the findings of our study are available from the corresponding author upon reasonable request.

ORCID

Hideyo Sato https://orcid.org/0000-0002-3732-7344

REFERENCES

1. Sato H, Tamba M, Ishii T, Bannai S. Cloning and expression of a plasma membrane cystine/glutamate exchange transporter composed of two distinct proteins. *J Biol Chem*. 1999;274:11455-11458.
2. Sato H, Tamba M, Kuriyama-Matsumura K, Okuno S, Bannai S. Molecular cloning and expression of human xCT, the light chain of amino acid transport system xc. *Antioxid Redox Signal*. 2000;2:665-671.

3. Bannai S. Exchange of cystine and glutamate across plasma membrane of human fibroblasts. *J Biol Chem*. 1986;261:2256-2263.
4. Kobayashi S, Sato M, Kasakoshi T, et al. Cystathionine is a novel substrate of cystine/glutamate transporter: implications for immune function. *J Biol Chem*. 2015;290:8778-8788.
5. Dixon SJ, Lemberg KM, Lamprecht MR, et al. Ferroptosis: an iron-dependent form of nonapoptotic cell death. *Cell*. 2012;149:1060-1072.
6. Stockwell BR, Friedmann Angeli JP, Bayir H, et al. Ferroptosis: a regulated cell death nexus linking metabolism, redox biology, and disease. *Cell*. 2017;171:273-285.
7. Friedmann Angeli JP, Krysko DV, Conrad M. Ferroptosis at the crossroads of cancer-acquired drug resistance and immune evasion. *Nat Rev Cancer*. 2019;19:405-414.
8. Jiang L, Kon N, Li T, et al. Ferroptosis as a p53-mediated activity during tumour suppression. *Nature*. 2015;520:57-62.
9. Zhang Y, Shi J, Liu X, et al. BAP1 links metabolic regulation of ferroptosis to tumour suppression. *Nat Cell Biol*. 2018;20:1181-1192.
10. Tarangelo A, Magtanong L, Bieging-Rolett KT, et al. p53 suppresses metabolic stress-induced Ferroptosis in cancer cells. *Cell Rep*. 2018;22:569-575.
11. Chen RS, Song YM, Zhou ZY, et al. Disruption of xCT inhibits cancer cell metastasis via the caveolin-1/beta-catenin pathway. *Oncogene*. 2009;28:599-609.
12. Bolli E, O'Rourke JP, Conti L, et al. A virus-like-particle immunotherapy targeting epitope-specific anti-xCT expressed on cancer stem cell inhibits the progression of metastatic cancer in vivo. *Onco Targets Ther*. 2018;7:e1408746.
13. Sato H, Shiiya A, Kimata M, et al. Redox imbalance in cystine/glutamate transporter-deficient mice. *J Biol Chem*. 2005;280:37423-37429.
14. Belloni PN, Carney DH, Nicolson GL. Organ-derived microvessel endothelial cells exhibit differential responsiveness to thrombin and other growth factors. *Microvasc Res*. 1992;43:20-45.
15. Mizushima S, Nagata S. pEF-BOS, a powerful mammalian expression vector. *Nucleic Acids Res*. 1990;18:5322.
16. Sato M, Kusumi R, Hamashima S, et al. The ferroptosis inducer erastin irreversibly inhibits system xc- and synergizes with cisplatin to increase cisplatin's cytotoxicity in cancer cells. *Sci Rep*. 2018;8:968.
17. Ingold I, Aichler M, Yefremova E, et al. Expression of a catalytically inactive mutant form of glutathione peroxidase 4 (Gpx4) confers a dominant-negative effect in male fertility. *J Biol Chem*. 2015;290:14668-14678.
18. Kohler G, Milstein C. Continuous cultures of fused cells secreting antibody of predefined specificity. *Nature*. 1975;256:495-497.
19. Doll S, Proneth B, Tyurina YY, et al. ACSL4 dictates ferroptosis sensitivity by shaping cellular lipid composition. *Nat Chem Biol*. 2017;13:91-98.
20. Kanda Y, Osaki M, Onuma K, et al. Amigo2-upregulation in tumour cells facilitates their attachment to liver endothelial cells resulting in liver metastases. *Sci Rep*. 2017;7:43567.
21. Liang CC, Park AY, Guan JL. In vitro scratch assay: a convenient and inexpensive method for analysis of cell migration in vitro. *Nat Protoc*. 2007;2:329-333.
22. Poste G, Doll J, Hart IR, Fidler IJ. In vitro selection of murine B16 melanoma variants with enhanced tissue-invasive properties. *Cancer Res*. 1980;40:1636-1644.
23. Ishii T, Bannai S, Sugita Y. Mechanism of growth stimulation of L1210 cells by 2-mercaptoethanol in vitro. Role of the mixed disulfide of 2-mercaptoethanol and cysteine. *J Biol Chem*. 1981;256:12387-12392.
24. Sasaki H, Sato H, Kuriyama-Matsumura K, et al. Electrophile response element-mediated induction of the cystine/glutamate exchange transporter gene expression. *J Biol Chem*. 2002;277:44765-44771.
25. Banjac A, Perisic T, Sato H, et al. The cystine/cysteine cycle: a redox cycle regulating susceptibility versus resistance to cell death. *Oncogene*. 2008;27:1618-1628.
26. Yang WS, SriRamaratnam R, Welsch ME, et al. Regulation of ferroptotic cancer cell death by GPX4. *Cell*. 2014;156:317-331.
27. Friedmann Angeli JP, Schneider M, Proneth B, et al. Inactivation of the ferroptosis regulator Gpx4 triggers acute renal failure in mice. *Nat Cell Biol*. 2014;16:1180-1191.
28. Dixon SJ, Patel DN, Welsch M, et al. Pharmacological inhibition of cystine-glutamate exchange induces endoplasmic reticulum stress and ferroptosis. *Elife*. 2014;3:e02523.
29. Onuma K, Suenaga Y, Sakaki R, et al. Development of a quantitative bioassay to assess preventive compounds against inflammation-based carcinogenesis. *Nitric Oxide*. 2011;25:183-194.
30. Polewski MD, Reveron-Thornton RF, Cherryholmes GA, Marinov GK, Aboody KS. SLC7A11 overexpression in Glioblastoma is associated with increased cancer stem cell-like properties. *Stem Cells Dev*. 2017;26:1236-1246.
31. Bannai S, Sato H, Ishii T, Taketani S. Enhancement of glutathione levels in mouse peritoneal macrophages by sodium arsenite, cadmium chloride and glucose/glucose oxidase. *Biochim Biophys Acta*. 1991;1092:175-179.
32. Sato H, Nomura S, Maebara K, Sato K, Tamba M, Bannai S. Transcriptional control of cystine/glutamate transporter gene by amino acid deprivation. *Biochem Biophys Res Commun*. 2004;325:109-116.
33. Koppula P, Zhang Y, Shi J, Li W, Gan B. The glutamate/cystine antiporter SLC7A11/xCT enhances cancer cell dependency on glucose by exporting glutamate. *J Biol Chem*. 2017;292:14240-14249.
34. Koppula P, Zhang Y, Zhuang L, Gan B. Amino acid transporter SLC7A11/xCT at the crossroads of regulating redox homeostasis and nutrient dependency of cancer. *Cancer Commun (Lond)*. 2018;38:12.
35. Talmadge JE, Fidler IJ. AACR centennial series: the biology of cancer metastasis: historical perspective. *Cancer Res*. 2010;70:5649-5669.
36. Bannai S, Sato H, Ishii T, Sugita Y. Induction of cystine transport activity in human fibroblasts by oxygen. *J Biol Chem*. 1989;264:18480-18484.
37. Stepulak A, Rola R, Polberg K, Ikonomidou C. Glutamate and its receptors in cancer. *J Neural Transm (Vienna)*. 2014;121:933-944.
38. Briggs KJ, Koivunen P, Cao S, et al. Paracrine induction of HIF by glutamate in breast cancer: EglN1 senses cysteine. *Cell*. 2016;166:126-139.
39. Lu H, Samanta D, Xiang L, et al. Chemotherapy triggers HIF-1-dependent glutathione synthesis and copper chelation that induces the breast cancer stem cell phenotype. *Proc Natl Acad Sci U S A*. 2015;112:E4600-E4609.
40. Wang Z, Dillon J, Gaillard ER. Antioxidant properties of melanin in retinal pigment epithelial cells. *Photochem Photobiol*. 2006;82:474-479.
41. Arensman MD, Yang XS, Leahy DM, et al. Cystine-glutamate antiporter xCT deficiency suppresses tumor growth while preserving antitumor immunity. *Proc Natl Acad Sci USA*. 2019;116:9533-9542.
42. Nabeyama A, Kurita A, Asano K, et al. xCT deficiency accelerates chemically induced tumorigenesis. *Proc Natl Acad Sci USA*. 2010;107:6436-6441.

SUPPORTING INFORMATION

Additional supporting information may be found online in the Supporting Information section at the end of this article.

How to cite this article: Sato M, Onuma K, Domon M, et al. Loss of the cystine/glutamate antiporter in melanoma abrogates tumor metastasis and markedly increases survival rates of mice. *Int. J. Cancer*. 2020;147:3224–3235. https://doi.org/10.1002/ijc.33262